ACS OMEGA

Open Access

http://pubs.acs.org/journal/acsodf

Article

Optimized Degradation of Doxycycline in Aqueous Systems Using Calcium Peroxide Nanoparticles via Response Surface Methodology

Nurul Nazihah Amerhaider Nuar,* Siti Nurul Ain Md Jamil, Thomas Shean Yaw Choong,* Syazana Ishami Mahadzir, Intan Diana Mat Azmi, Mohd Salahuddin Mohd Basri, and Mohamad Rezi Abdul Hamid

Cite This: *ACS Omega* 2025, 10, 10205−10219

Read Online

ACCESS | Metrics & More | Article Recommendations | Supporting Information

ABSTRACT: The presence of antibiotic residues in aqueous systems, particularly doxycycline (DOX), is harmful to the environment and public health. In this study, dextran-coated calcium peroxide nanoparticles (DEX@nCPs(DEX)), Fe(II), and oxalic acid (OA) were combined to improve the heterogeneous Fenton-like degradation of DOX. X-ray photoelectron spectroscopy (XPS) demonstrated the successful synthesis of DEX@nCPs-(DEX), showing the presence of Ca, O, and C functional groups associated with dextran. Using response surface methodology with a central composite design (RSM-CCD), the optimal conditions (DEX@nCPs(DEX) dosage: 2 g/L, pH: 5, contact time: 420 min) achieved 90% DOX removal, which was 20% higher than using DEX@nCPs(DEX)/Fe(II) alone. The degradation process followed first-order kinetics with a rate constant of k_1 = 0.0047 min^{-1}. Model validation showed high predictive accuracy (R^2 = 0.996; adjusted R^2 = 0.987). Scavenger and photoluminescence analyses revealed hydroxyl radicals (•OH) to be the primary reactive species, accounting for over 80% of the degradation activity. The DEX@nCPs(DEX)/Fe(II)/OA system offers a promising approach for mitigating pharmaceutical pollutants in water, contributing to more sustainable environmental management practices.

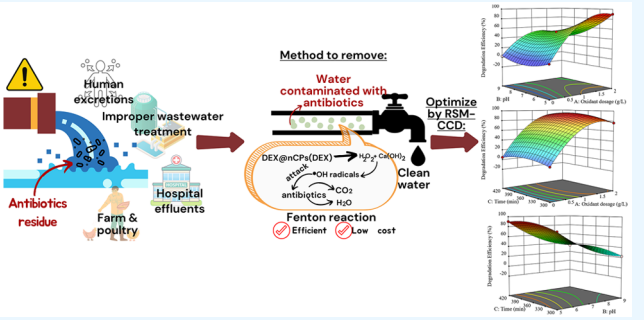

INTRODUCTION

Doxycycline (DOX), a tetracycline antibiotic, is widely used in human and veterinary medicine. It is a broad-spectrum antibiotic that works against a variety of Gram-positive and Gram-negative bacteria.[1] Despite its widespread use and effectiveness, the presence of DOX in the environment has raised serious concerns. The presence of DOX in the environment can promote the development and spread of antibiotic resistance in bacterial populations, thereby posing a serious threat to public health.[2] To mitigate the potential negative effects of DOX, effective strategies for its removal from wastewater and the environment must be developed.

Several techniques have been studied for the treatment of antibiotic-polluted wastewater, including biological processes, adsorption methods, membrane filtration systems, and advanced oxidation processes (AOPs), which have been extensively utilized for the elimination of persistent contaminants, such as antibiotics, from water.[3−5] Fenton reaction produces highly reactive hydroxyl radicals (•OH) via the catalytic breakdown of hydrogen peroxide (H_2O_2) by iron ions.[6,7] However, this homogeneous Fenton oxidation process is hindered by significant issues, including excessive iron sludge production, pH sensitivity requiring a narrow acidic range (pH 2−4), and risk of secondary pollution from residual iron or unreacted substances.[8,9]

To overcome these constraints, researchers have progressively turned to heterogeneous Fenton-like systems, in which iron is immobilized on or within solid assistance.[10] These methods can decrease iron leaching, increase oxidation efficiency, and reduce sludge formation.[11,12] In contrast to previous heterogeneous Fenton-based systems, our study presented a synergistic approach utilizing DEX@nCPs(DEX) as an oxidant, Fe(II) as catalyst, and OA as a chelating agent for iron cycling.[13,14] The dextran coating improved the stability and dispersion of the nCPs, ensuring a controlled H_2O_2 release.[15,16] Additionally, the chelating effect of OA on Fe prevents precipitation and forms ferric-oxalate complexes, which can be reduced to Fe(II), thereby enhancing •OH radical production.[17,18] As a result, this integrated system achieves superior removal of targeted antibiotics compared to

Received: October 17, 2024
Revised: February 7, 2025
Accepted: February 13, 2025
Published: March 7, 2025

traditional Fenton processes, offering a robust and scalable solution for advanced water treatment applications.

Calcium oxide (CaO) and calcium hydroxide ($Ca(OH)_2$) were used as AOPs for pollutant reduction. Alrozi et al.[19] demonstrated a 97.0% degradation efficiency for acid orange II dye using $CaCuFeO_3$ perovskite. This demonstrates the efficacy of calcium in increasing the catalytic activity. Xie et al.[20] found that the $Co_2Ca_1Al_1$-LDO/PAA system removed micropollutants with efficiencies ranging from 90.4 to 100.0%, with organic radicals playing a dominant role in the degradation process. This highlights the potential of calcium in layered double oxides for AOPs. Although these calcium-based catalysts perform admirably in pollutant degradation, their use frequently necessitates the addition of oxidants or activators, which can complicate and increase the cost of treatment procedures. Calcium peroxide (CaO_2) is unique because it can act as both an oxidant and source of calcium ions. When CaO_2 comes in contact with water, it releases H_2O_2, resulting in reactive oxygen species that can help degrade pollutants.[21,22] This eliminates the need for external oxidants, simplifies the treatment process.

To improve DOX degradation in aqueous systems, this study used response surface methodology with a central composite design (RSM-CCD) for optimization. The RSM-CCD is a well-known and effective experimental design approach that allows researchers to create models, evaluate the effects of various factors, and identify the optimal conditions for the desired outcomes.[23] This method has significant advantages over traditional one-factor-at-a-time (OFAT) approaches because it allows for the simultaneous manipulation of multiple independent variables, improves the understanding of interactions, and reduces the number of experiments required, thus saving time and money.[24,25] RSM-CCD has been successfully applied in various wastewater treatment processes, including the optimization of parameters for removing harmful dyes and pollutants from different effluents.[26,27] These applications demonstrate the adaptability and efficacy of the RSM-CCD for increasing the efficiency and sustainability of wastewater treatment processes.

In this study, the optimization and efficiency of the DOX degradation process were investigated using a two-pronged approach: application of RSM-CCD for process optimization and addition of a chelating agent in Fenton-like reactions to improve the degradation efficiency. While the potential of DOX degradation has been investigated, research into optimizing the reaction parameters and understanding the mechanisms of Fenton-like degradation is limited. To address this, the study evaluated parameter ranges for optimization, determined the optimal reaction conditions for increased DOX degradation efficiency, examined the reaction kinetics, and proposed potential degradation mechanisms. Furthermore, this research aims to advance long-term and effective strategies for minimizing antibiotic pollution by improving the degradation process and optimizing the operational parameters.

2. MATERIALS AND METHODS

2.1. Materials. Dextran-coated calcium peroxide nanoparticles (DEX@nCPs(DEX)) was synthesized utilizing analytical-grade reagents. Oxalic acid (OA), Fe(II) sulfate, and additional reagents were obtained from Sigma-Aldrich (Malaysia) and utilized without further purification. All the glassware and reaction vessels were meticulously cleaned to avoid contamination.

Details regarding the materials and analytical procedures are provided in the Supporting Information (Texts S1−S3).

2.2. Synthesis of Dextran-Coated Calcium Peroxide Nanoparticles. Initially, calcium peroxide was synthesized using dextran as a stabilizing agent and labeled as (nCPs-(DEX)). Subsequently, dextran-coated calcium peroxide nanoparticles (DEX@nCPs(DEX)) were obtained by dextran coating the synthesized nCPs(DEX), as previously described in our published article.[21] The details of the synthesis are provided in the Supporting Information (Text S2). We highlight the extended benefits of DEX@nCPs(DEX) in wastewater remediation owing to the controlled release of H_2O_2 (Figure S1).

2.3. Experimental Procedures. All experiments were carried out in a 250 mL Erlenmeyer flask at 25 ± 2 °C with a constant stirring rate of 150 rpm. DOX (10 mg/L) was prepared daily for all the experiments. This concentration was chosen to facilitate the study of residual DOX concentrations, despite being higher than typical environmental levels. All degradation reactions were carried out in a phosphate buffer to maintain the pH, as DEX@nCPs(DEX) have a tendency to shift the pH toward alkalinity. To start the reaction, DEX@nCPs(DEX) and other chemicals were dissolved in a flask. Control tests were performed without the addition of DEX@nCPs(DEX). Samples (4 mL) were collected at regular intervals, quenched with 2 M Na_2SO_3, centrifuged (4000 rpm, 5 min), and filtered (0.22 μm) before analysis. A calibration curve was used to convert the UV−vis absorbance measurements to DOX concentrations (see Figure S2). Figure 1 shows a schematic of the DOX degradation study.

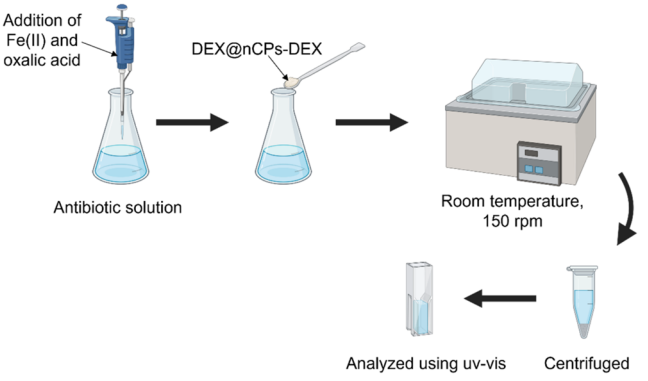

Figure 1. Schematic diagram of DOX degradation studies using the DEX@nCPs(DEX)/Fe(II)/OA system. Created using Biorender.com.

Chemical oxygen demand (COD) values were determined using the dichromate digestion-colorimetric method (Lovibond thermoreactor RD125, DR/890 Portable colorimeter). The reactive oxygen species (ROS) responsible for DOX degradation were determined using radical scavenging and photoluminescence studies.[28] Excess *tert*-butyl alcohol (TBA) and chloroform (CF) were added to scavenge hydroxyl ($^{\bullet}OH$) and superoxide ($^{\bullet}O_2^-$) radicals.

2.4. Optimization of Reaction Parameters Using RSM-CCD. The influence of DEX@nCPs(DEX) dosage, solution pH, and contact time on DOX degradation efficiency was examined using response surface methodology with a central composite design (RSM-CCD) in the Design Expert software (version 13.0). A face-centered CCD model was employed,

https://doi.org/10.1021/acsomega.4c09460
ACS Omega 2025, 10, 10205−10219

with three levels (−1, 0, +1) assigned to each parameter. The coded levels for each independent variable, oxidant dosage (0, 1, and 2 g/L), pH (5, 7, and 9), and contact time (300, 360, and 420 min), were selected based on preliminary studies (Table 1). The experimental matrix and response data were

Table 1. Ranges and Levels of Independent Variables in the Experiment

		Range and level		
Independent variables	Symbol	−1	0	1
Oxidant dosage (g/L)	A	0	1	2
pH	B	5	7	9
Contact time (min)	C	300	360	420

analyzed to develop a quadratic model predicting the degradation efficiency, and ANOVA was used to assess the significance and accuracy of the model.

The model used to predict the optimum parameters is represented by the quadratic equation in eq 1

$$Y = \beta_0 + \beta_1 A + \beta_2 B + \beta_3 C + \beta_{11} A^2 + \beta_{22} B^2 + \beta_{33} C^2 + \beta_{12} AB + \beta_{13} AC + \beta_{23} BC + \varepsilon \quad (1)$$

where Y is the dependent variable (DOX degradation efficiency); A, B and C represent the effects of the independent variables; AB, AC and BC are the interaction effects between variables; A^2, B^2 and C^2 are the square effects of the variables; β_o represents a constant; β_1, β_2 and β_3 are the linear coefficients; β_{12}, β_{13} and β_{23} are the interaction coefficients; and ε represents the residual term.[29] The relationship between the independent parameters and their effects on DOX degradation efficiency is depicted in two- and three-dimensional graphs.

2.5. Kinetic Analysis. The degradation kinetics were evaluated by fitting the concentration data to first- and second-order models. Rate constants were derived from linearized equations and correlation coefficients (R_2) were calculated to determine the best-fitting model. The optimal kinetic model for DOX degradation in this system was further confirmed by plotting the residuals and analyzing the reaction rates under varying concentrations of DEX@nCPs(DEX).

2.6. Characterizations. To confirm the successful synthesis of DEX@nCPs(DEX), the samples were characterized using X-ray Photoelectron Spectroscopy (XPS). All details are provided in the Supporting Information. To elucidate the degradation pathway, the precipitates formed during degradation were analyzed using Fourier transform infrared (FTIR)

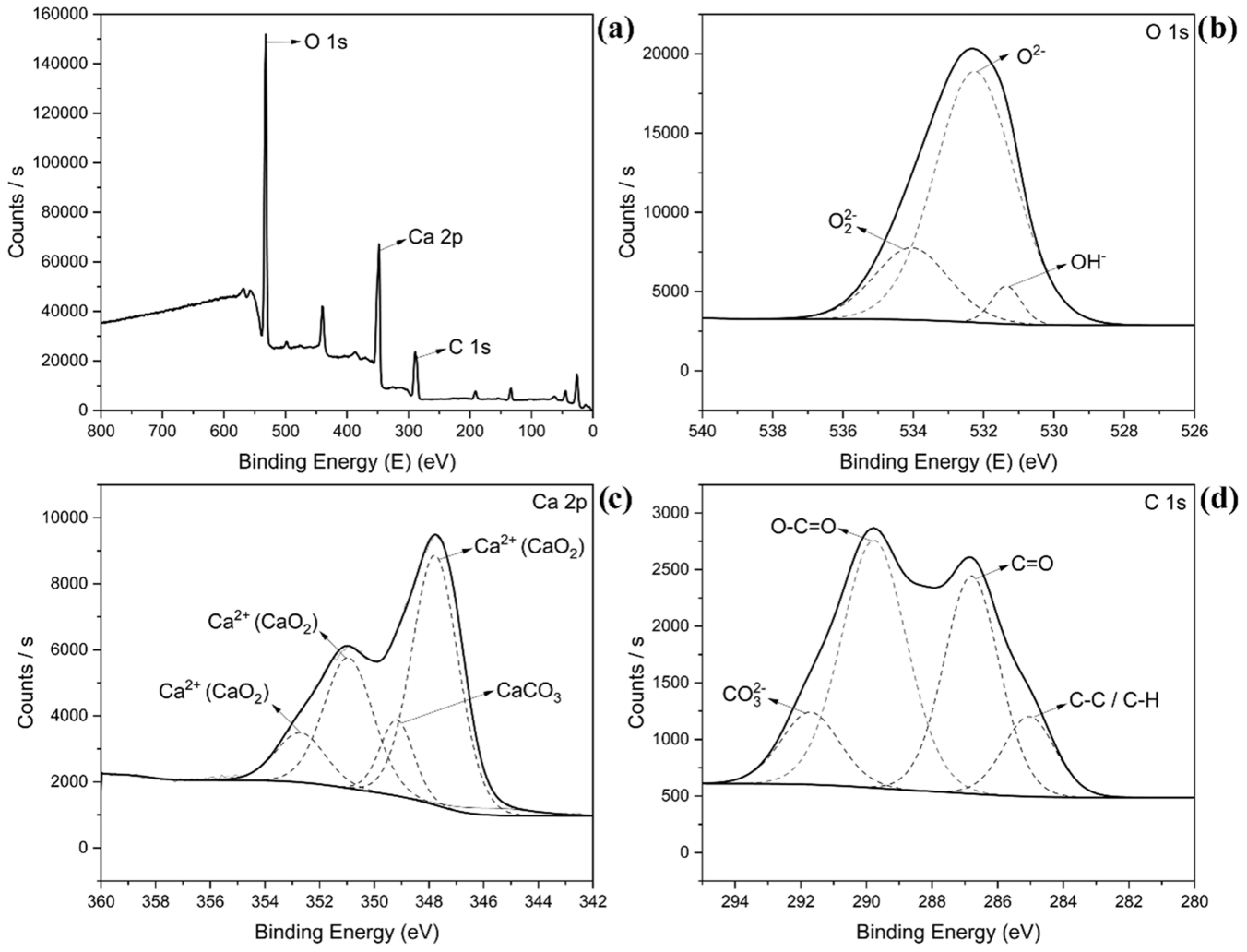

Figure 2. (a) XPS survey spectrum and high-resolution spectra (b) O 1s, (c) Ca 2p, and (d) C 1s of DEX@nCPs(DEX).

https://doi.org/10.1021/acsomega.4c09460
ACS Omega 2025, 10, 10205−10219

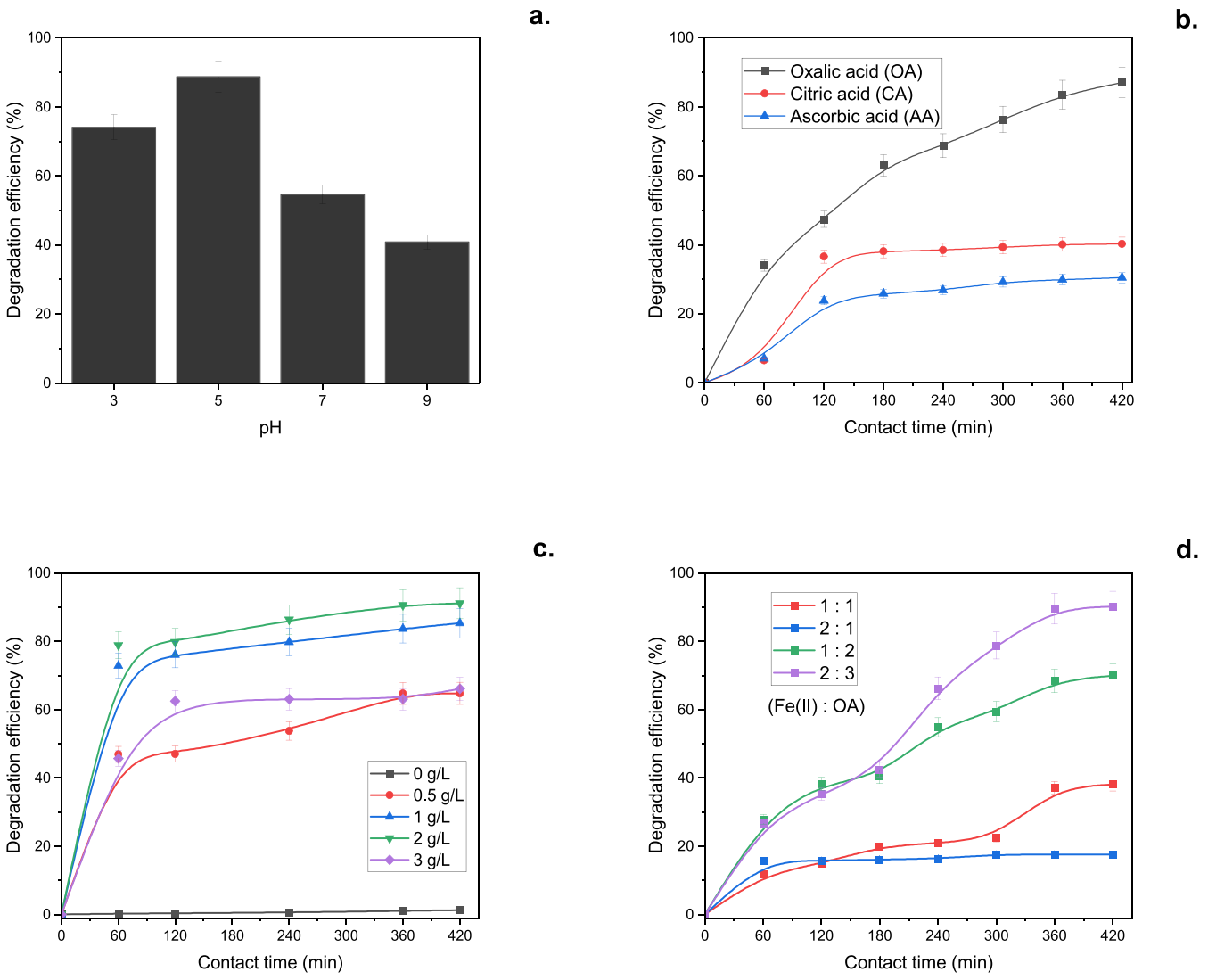

Figure 3. Effects of (a) initial pH, (b) type of chelating agents, (c) initial DEX@nCPs(DEX) dosage, and (d) Fe(II): OA molar ratio on DOX degradation efficiency. The experimental conditions were [DOX] = 10 mg/L, room temperature, and pH = 5 ± 0.2 in phosphate buffer solution (except for (a)).

spectroscopy, scanning electron microscopy (SEM), and energy-dispersive X-ray (EDX) analysis. FTIR spectra provided information on functional groups involved in the degradation process, while SEM and EDX analyses offered insights into the morphology and elemental composition of precipitates. Photoluminescence and radical scavenging tests confirmed the involvement of hydroxyl radicals ($^{\bullet}OH$) as the primary active species in the degradation process.

3. RESULTS AND DISCUSSIONS

3.1. X-ray Photoelectron Spectroscopy. The XPS spectrum analysis (Figure 2a) validates the existence of O, Ca, and C elements in DEX@nCPs(DEX), confirming the successful synthesis of dextran-coated calcium peroxide nanoparticles. The high-resolution O 1s spectrum (Figure 2b) revealed three distinct peaks at 531 eV for lattice O_2, 532.5 eV for dextran-associated O_2, and 534 eV for peroxide O_2, thereby confirming the structure of CaO_2 and indicating contributions from the dextran coating and possible impurities.[30,31]

In the Ca 2p spectrum (Figure 2c), peaks near 347.8 eV (Ca 2p3/2) and 351.0 eV (Ca 2p1/2) validate calcium's presence in CaO_2, while an additional peak around 349 eV indicates minor carbonate; the C 1s spectrum (Figure 2d) reveals the dextran coating's chemical structure with peaks at approximately 284.8 eV (C−C/C−H) and 285.5 eV (C−O), alongside peaks at 288.5 and 290 eV that suggest oxidized carbon species and carbonate impurities, respectively.[30−33]

3.2. Enhanced Degradation Studies of DOX with the Addition of Chelating Agent. Before choosing the correct parameter range in the RSM-CCD studies, several parameters were evaluated, including the effect of the initial pH, different types of chelating agents to enhance the degradation efficiency, effect of the initial oxidant dosage, and effect of the Fe(II)/OA molar ratio. This degradation study is important to ensure that the range selected in later optimization studies is correct, thus making optimization studies effective and efficient.

3.2.1. Effect of Initial pH. Figure 3a shows the DOX degradation trend under different initial pH conditions. The DOX degradation efficiency increased from 66 to 90% when the pH increased from 3 to 5 (± 0.2), and declined to 40% as

https://doi.org/10.1021/acsomega.4c09460
ACS Omega 2025, 10, 10205−10219

the pH was increased to 11.0. The optimal pH for DOX degradation by the synergistic DEX@nCPs(DEX)/Fe(II)/OA system was approximately 5 ± 0.2. As reported in our previous study, for Fenton reactions without chelators, a pH of 3 ± 0.2 allows for optimal iron solubility and •OH radical generation.[21] However, the addition of oxalic acid shifted the degradation efficiency to a less acidic pH with an optimal pH of 5 ± 0.2. A previous study by Messele et al.[34] emphasized the influence of chelators on the optimum pH in Fenton-like systems, highlighting their ability to alter the speciation and solubility of Fe.

In addition, the solubility of DEX@nCPs(DEX) and generation of H_2O_2 in the DEX@nCPs(DEX)/Fe(II)/OA system were significantly influenced by the pH of the solution. At low pH levels, DEX@nCPs(DEX) primarily released H_2O_2, whereas as the pH increased, its solubility decreased, and $Ca(OH)_2$ and O_2 were predominantly produced (eqs 2 and 3).[35,36] Therefore, maintaining the pH of the solution in the buffer can affect the rate of H_2O_2 release and DOX degradation efficiency

$$\text{DEX@nCPs(DEX)} + 2H_2O \rightarrow H_2O_2 + Ca(OH)_2 \quad (2)$$

$$\text{DEX@nCPs(DEX)} + H_2O \rightarrow 0.5O_2 + Ca(OH)_2 \quad (3)$$

3.2.2. Effect of Different Chelating Agent on DOX Degradation Efficiency. This study examined the effects of three chelating agents, oxalic acid (OA), citric acid (CA), and ascorbic acid (AA), on the degradation of doxycycline (DOX) in a DEX@nCPs(DEX)/Fe(II) system at pH 5. As illustrated in Figure 3b, OA exhibited a significantly higher degradation efficiency (87%) within 420 min than CA (40%) and AA (31%). The differences in DOX degradation efficiency were attributed to the chelating strengths and molecular structures of the compounds.[37]

The larger size and presence of multiple functional groups in CA result in steric hindrance, which hinders the ability of the molecule to efficiently bind to Fe(II), unlike the simpler structure of OA. In contrast, a single binding site of AA leads to weaker monodentate chelation and less stable complexes. These results are consistent with the study by Pignatello et al.[38] who demonstrated different levels of degradation of pentachlorophenol in Fenton-like reactions based on the chelating agent used, with the order of efficiency as follows: OA > EDTA > carboxymethyl-β-cyclodextrin (CMCD) > CA > TA > succinic acid > no chelating agent.[38] This highlights the importance of choosing suitable chelating agents to optimize the pollutant removal efficiency.

Additionally, OA formed a stable complex with Fe(II) in the form of a ferric-oxalate complex (eq 4). The iron-oxalate complex reacts with H_2O_2 produced by DEX@nCPs(DEX) to form •OH radicals. These radicals are highly reactive and can oxidize organic pollutants (eq 5). In addition, OA can regenerate Fe(II) from Fe(III), which helps in the continuous generation of •OH radicals by decomposing H_2O_2 (eq 6). This improvement highlights the promising use of OA for optimizing Fenton-like reactions for the efficient degradation of antibiotics

$$\text{Fe(II)} + (C_2O_4)^{2-} \rightarrow \text{Fe(II)} - C_2O_4^{2-} \quad (4)$$

$$\text{Fe(II)} - C_2O_4^{2-} + H_2O_2 \rightarrow \text{Fe(III)} - C_2O_4^{+} + {}^{\bullet}OH + OH^{-} \quad (5)$$

$$\text{Fe(III)} - C_2O_4^{+} + H_2O_2 \rightarrow \text{Fe(II)} - C_2O_4^{2-} + 2H^{+} \quad (6)$$

3.2.3. Effect of Initial Oxidant Dosage. To determine the optimum dosage of DEX@nCPs(DEX) for DOX degradation, degradation studies were conducted at a constant molar ratio of Fe(II)/OA (2:3) using different DEX@nCPs(DEX) dosages. As shown in Figure 3c, it could be clearly seen that the degradation of DOX was low when 0.5 and 3 g/L was used. In the absence of DEX@nCPs(DEX), the degradation efficiency was negligible. A remarkable increase can be seen from 60 to 90% within 420 min when the oxidant dosage increases from 0.5 to 2 g/L. Increasing the amount of DEX@nCPs(DEX) can result in increased generation of H_2O_2, which leads to more •OH radicals degrading DOX. However, a further increase in oxidant dosage to 3 g/L decreased the degradation efficiency to 60%. This was probably because of the overgeneration of H_2O_2 from the excess dosage of DEX@nCPs(DEX), which could scavenge the reactive species in the system. This hindered the degradation of DOX, thereby decreasing its degradation efficiency.

3.2.4. Effect of Fe(II): OA Molar Ratio. Experiments were conducted to determine the optimal Fe(II): OA molar ratios of 1:1, 2:1, 1:2, and 2:3 (Figure 3d). As can be seen from the results, when the Fe(II) dosages were the same or higher than those of OA, DOX degradation efficiency decreased. When the OA dosage was higher than that of Fe(II), DOX degradation efficiency increased. The presence of excess chelate was found to enhance the efficiency of the Fe(II): OA system in degrading DOX.[39] The addition of an appropriate amount of Fe(II): OA enhanced the Fenton-like reaction by the complexation of Fe and OA, improving DOX removal, which can be quantified in several ways. First, The Fe(II)-OA complexes could facilitate electron transfer between Fe(II) and Fe(III) through the coordination between Fe(II)/Fe(III) and OA, promoting the recycling of Fe(II) and reducing iron precipitation as $Fe(OH)_3$ (eq 7). Second, by minimizing $Fe(OH)_3$ formation through recomplexation, the excess chelate reduces the scavenging of •OH radicals, enhancing their utilization and further improving degradation efficiency.

3.3. Response Surface Model Analysis. *3.3.1. Regression Analysis.* The experiment was performed randomly according to the design matrix of the RSM-CCD matrix generated using Design Expert software (version 13.0). Fifteen experiments with different combinations of oxidant dosage, pH, and contact time showed significant effects on DOX degradation efficiency. The results presented in Table S1 show the observed and predicted responses, with considerable variations in DOX degradation efficiency. The experimental results of the RSM-CCD study showed that the maximum observed degradation efficiency of DOX was 90.1% at an oxidant dosage of 2 g/L, a pH of 5, and a contact time of 420 min (run 9). The experiment without the DEX@nCPs(DEX) dosage (0 g/L), which acted as a control, resulted in negligible DOX degradation efficiency (2.5%).

Multiple regression model analyses were performed using various methods for model selection with a confidence interval of 95%. Based on the results in Table S1, the experimental data were strongly correlated with the second-order polynomial model. The model successfully described the correlation between initial oxidant dosage, solution pH, and contact time. The relationship between these parameters is expressed in terms of the coded factors in eq 7

https://doi.org/10.1021/acsomega.4c09460
ACS Omega 2025, 10, 10205−10219

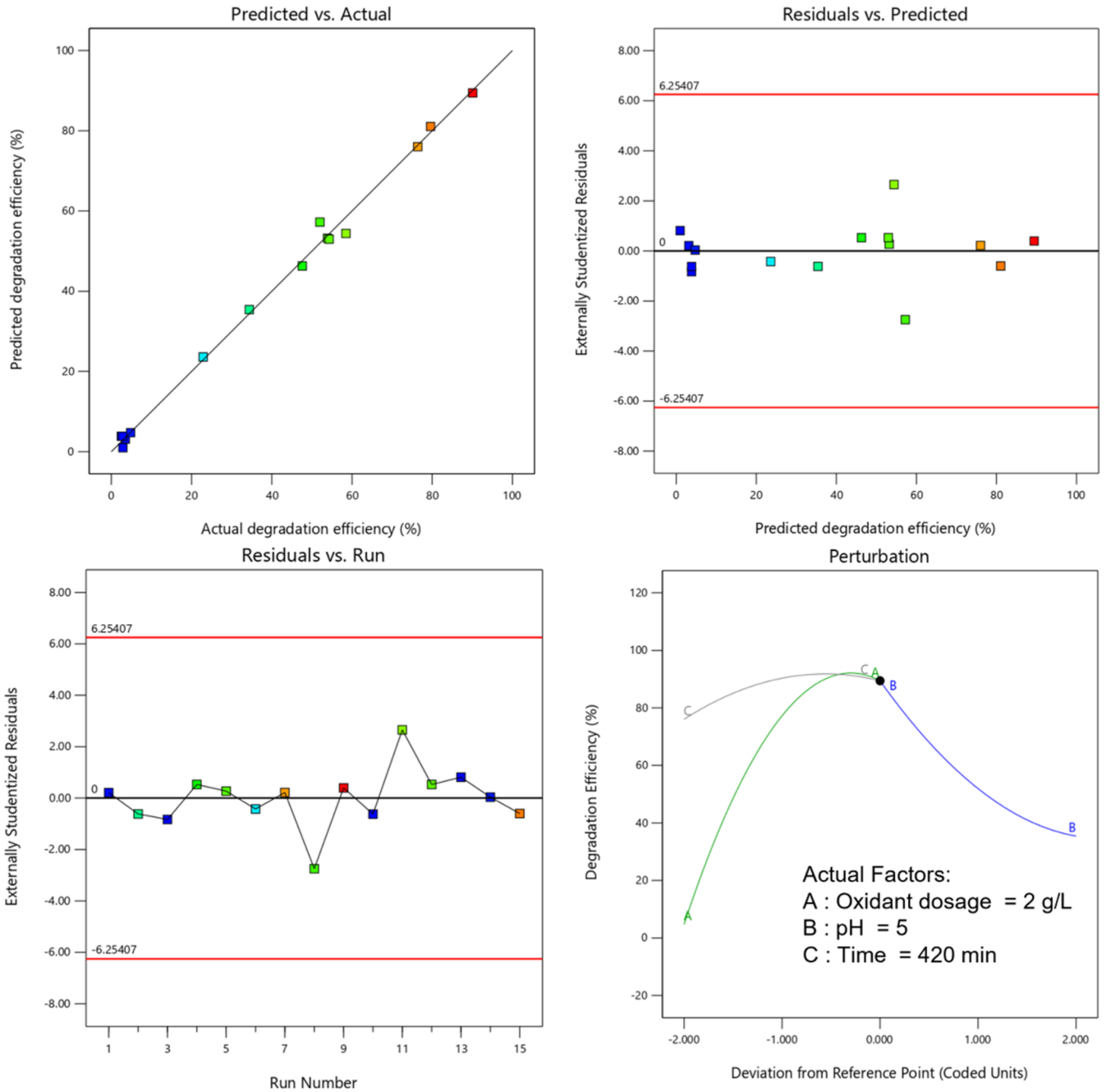

Figure 4. Diagnostic plots for (a) predicted versus actual data, (b) externally studentized residuals versus predicted values, (c) externally studentized residuals versus run numbers, and (d) perturbation plots.

$$Y = 57.24 + 26.12A - 13.33B + 3.35C - 13.27AB + 2.95AC - 0.40BC - 30.14A^2 - 10.51B^2 - 7.59C^2 \quad (7)$$

where Y is the DOX degradation efficiency (%), A is the oxidant dosage (g/L), B is the pH of the solution, and C is the contact time (min). The model equation showed that all three variables had significant effects on DOX degradation, as represented by either the negative or positive coefficients. This suggests that optimal degradation efficiency of DOX can be achieved by maximizing the oxidant dosage and contact time while minimizing the pH of the solution.[40]

The strong correlation between the predicted and actual DOX degradation efficiencies (Figure 4a) demonstrated the reliability of the developed predictive model.[41] The small difference between the two data sets indicated that the model accurately represented the behavior of the system. The agreement between the predicted and observed results also confirmed the ability of the model to estimate the interactions between the independent variables (oxidant dosage, pH, and contact time) and dependent variable (DOX degradation efficiency). The normality plot of the externally studentized residuals (Figure 4b,c) further supports the reliability of the response surface model, as the standard residuals were within the range of ±6.3. The normality plot of the externally studentized residuals showed that the model errors were normally distributed and independent.[42] This confirmed the reliability of the model and the absence of data errors. The

https://doi.org/10.1021/acsomega.4c09460
ACS Omega 2025, 10, 10205−10219

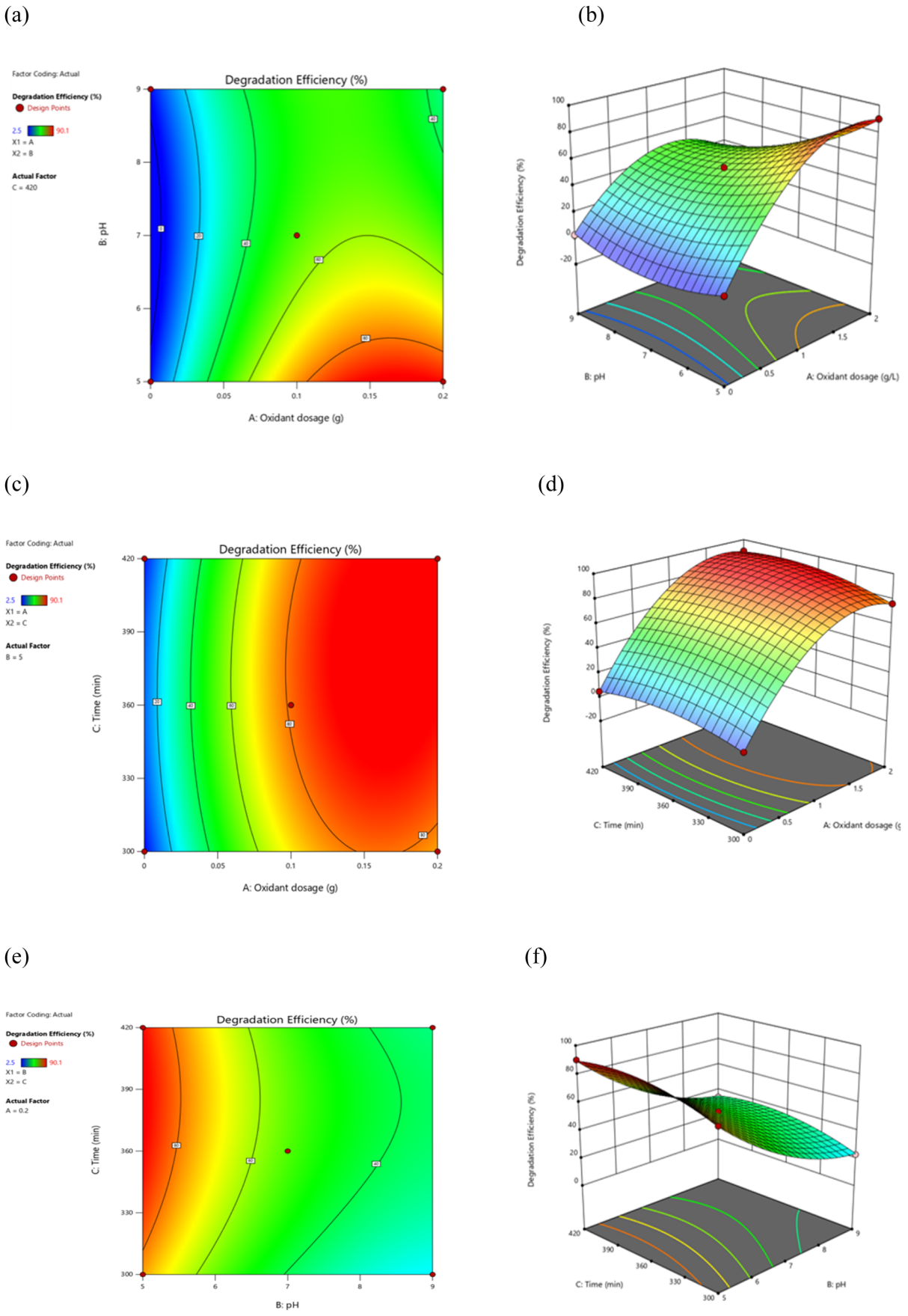

Figure 5. Interactions between (a, b) oxidant dosage and pH; (c, d) oxidant dosage and contact time; and (e, f) pH and contact time for DOX degradation efficiency in 2D contour plots and 3D response surfaces.

https://doi.org/10.1021/acsomega.4c09460
ACS Omega 2025, 10, 10205−10219

perturbation plot in Figure 4d illustrates the sensitivity of DOX degradation to the three factors within the designated design space, specifically under the optimal run conditions. The sharp curve indicates that small modifications of these parameters can significantly influence the efficiency of DOX degradation.[43]

3.3.2. Analysis of Variance (ANOVA). The ANOVA results for the quadratic model (eq 7) are listed in Table S2. The coefficient of determination fits the data well, with a high R^2 value of 0.9956 and an adjusted R^2 value of 0.9877, indicating that it can accurately predict DOX degradation efficiency. A low coefficient of variation (C.V) of 8.79% suggests that the model has low variability and is robust. According to Wu et al.,[44] C.V must not exceed 10% for the proposed model to be considered adequate. Furthermore, a strong correlation between the experimental data and the predicted model was achieved when the precision residual sum of squares (PRESS) was greater than four.[42] Therefore, a PRESS value of 312.25 was acceptable for the proposed quadratic model.

The statistical significance of the coefficient terms was assessed by analyzing the *p*-values ($p < 0.05$) and *F*-values, which showed that the model was highly significant, as indicated by the high *F*-value = 125.54 and low p-value (<0.0001). For the main effects, oxidant dosage (A) had a highly significant effect on DOX degradation efficiency (*F*-value = 578.10, $p < 0.0001$), followed by pH (B) (*F*-value = 150.56, $p < 0.0001$), whereas contact time (*C*) had a slightly lower but still significant effect (*F*-value = 9.51, $p = 0.0274$). Furthermore, the interactions between the oxidant dosage (*A*) and pH (*B*) had a significant effect compared to others, as shown by its high *F*-value of 119.46 and $p = 0.0001$. The order of the independent variables for enhancing DOX degradation efficiency was $A > B > C$, whereas the order of the interaction variables was $AB > AC > BC$.

3.3.3. Interactive Effects of Parameters. The combined impact of oxidant dosage and pH on the efficiency of DOX degradation at a consistent contact time of 420 min was illustrated using both two dimensional (2D) contour plots and a three dimensional (3D) response surface (Figure 5a,b). The graph shows that, when the oxidant dosage was low, the degradation efficiency decreased as the pH of the solution increased. Conversely, when the amount of oxidant was higher, the degradation efficiency increased as the pH of the solution decreased. This is because increasing the oxidant dosage increases the number of $^{\bullet}OH$ radicals available for DOX degradation. This trend is consistent with the results of previous studies on the degradation of other pollutants using nCPs. According to Vijuksungsith et al.,[45] the efficiency of oxytetracycline removal increased with higher dosages of CaO_2 nanoparticle-FGD, while Hung et al.[46] reported that the removal efficiency of 4-nonylphenol increased with higher oxidant dosages.

Figure 5c,5d show the interactive effects of oxidant dosage and contact time on DOX degradation efficiency at a constant oxidant dosage of 2 g/L. Increasing the oxidant dosage increased the number of $^{\bullet}OH$ radicals available to degrade antibiotic molecules. Without DEX@nCPs(DEX), minimal degradation (<10%) was observed, indicating that the DEX@nCPs(DEX) played an important role in the degradation process. A longer contact time gives $^{\bullet}OH$ radicals more time to interact with antibiotic molecules and initiate the degradation processes. It is also worth noting that the degradation efficiency can occur at extended contact times depending on the availability of $^{\bullet}OH$ radicals.[47,48] Therefore, chelation is crucial so that $^{\bullet}OH$ radicals are available throughout the extended contact time.

The effects of the pH and contact time on the efficiency of DOX degradation at a fixed oxidant dosage of 2 g/L are shown in Figure 5e,5f. The graph indicates that, at low pH levels, the removal efficiency increased as the contact time increased, whereas at higher pH levels, the degradation efficiency decreased as the contact time increased. This is consistent with the typical Fenton-like process, which is most effective in acidic environments.[49] The pH of the solution affects the Fenton-like process in several ways. Under acidic conditions, DEX@nCPs(DEX) exhibited a strong capacity to release H_2O_2 (eq 2). However, as the pH increased, DEX@nCPs(DEX) released O_2, as shown in eq 3.[50,51] In addition, an increase in the pH promoted the precipitation of Fe(II) into Fe(III), which inhibited the generation of $^{\bullet}OH$ radicals.[52] A lower pH is generally better for Fenton-like reactions because it favors the formation of $^{\bullet}OH$ radicals and inhibits their scavenging by other species.[50] Increasing the contact time increases the time for which the $^{\bullet}OH$ radicals react with DOX, which increases the DOX degradation efficiency. Mohagheghian et al.[41] also reported that maximum degradation of diazinon was achieved by lowering the pH with increasing contact time.

3.3.4. Verification Experiments of DOX Degradation. The data displayed in Table S1 demonstrate that the results were dependent on the specific experimental conditions selected. Therefore, it is essential to optimize the process to identify the optimal settings that result in the highest possible response. To accomplish this, a numerical optimization process was performed using Design Expert 13.0. The parameter for determining the optimum conditions that showed the highest response was established as the desirability function, which ranges from 0.0 1.0. A desirability function value approaching 1.0, signifies that the conditions have been optimized to achieve the highest possible response.[53]

The following ranges were used to optimize oxidant dosage, pH, and contact time: oxidant dosage (0−2 g/L), pH (5), and contact time (300−420 min). The shape of the desirability function was determined by setting both the upper and lower weights to 1. Table S3 presents a comprehensive list of criteria employed to determine the overall desirability function. To accomplish the optimization objectives, the software performed the search at a random starting point and advanced along the steepest slope until it reached its maximum.[54,55] As shown in Figure S3, the numerical optimization process identified a point at which the desirability function achieved a value of 1, indicating the optimal local maximum of the ramp desirability function for each independent variable. The optimal conditions for oxidant dosage, pH, and contact time were determined to be 2 g/L, pH5, 420 min, respectively.

Under these conditions, the software predicted a maximum DOX degradation efficiency of 89.4% (Table S4). The average experimental efficiency of DOX degradation was 85.6%, which was close to the predicted value, and the COD concentration decreased from 165 to 23 mg/L over 420 min (Figure 6). The accuracy and reliability of the model are validated by the close agreement between the predicted and experimental results, underscoring the importance of predictive software in environmental engineering, particularly for the optimization of wastewater treatment processes.

To provide a context for the degradation efficiency of DEX@nCPs (DEX) in this study, Table 2 highlights relevant findings from the literature on the degradation of various

https://doi.org/10.1021/acsomega.4c09460
ACS Omega 2025, 10, 10205−10219

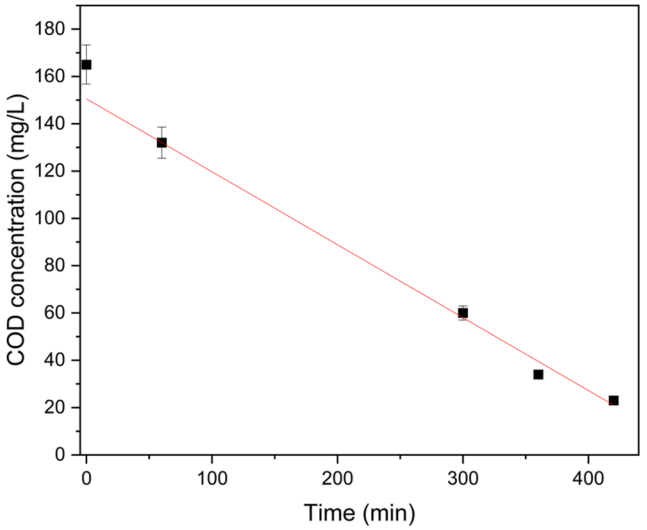

Figure 6. Total COD removal after 420 min using the predicted optimal conditions.

antibiotics using calcium-based or nanocalcium peroxide (nCPs) materials. Xu et al.[56] demonstrated an excellent 99.2% degradation efficiency for tetracyclines using ultrasonic waves and nCPs. Bembibre et al.[57] reported 99.2% efficiency in tetracycline degradation with a photocatalytic method with Ca-based nanoparticles. However, these methods frequently require specific energy inputs or light radiation, limiting their scalability. In contrast, Xiang et al.[58] used ozone with nCPs for sulfamethoxazole degradation and achieved a reduced effectiveness of 73.9%. This highlights the challenges of the oxidant consumption and reaction kinetics. Under optimal conditions, the Fenton-like degradation approach with DEX@nCPs(DEX) achieved 90.1% degradation efficiency for doxycycline. Although slightly less efficient than the photocatalytic or ultrasonic approaches, this method offers significant advantages in terms of simplicity, scalability, and synergistic improvement via Fe(II) cycling and oxalic acid as a chelating agent.

3.3.5. Kinetic Studies. DOX degradation efficiency was modeled using first-order (Figure 7a) and second-order kinetic models (Figure 7b) under the optimal conditions proposed by RSM-CCD, as shown in. The degradation experiment was performed by varying the contact time from 0 to 420 min. The study found that the first-order model provided a better fit, as demonstrated by the high correlation coefficient (R^2 = 0.9975), suggesting reliable experimental data, compared to the second-order model, which showed a lower correlation coefficient (R^2 = 0.9268). The rate constant (k_1) for DOX degradation determined in this study (0.0047 min) is comparable to that reported in other studies on the degradation of DOX. Sierra et al.[59] reported a rate constant (k_1) of 0.1265 min^{-1} for DOX degradation using simulated sunlight and H_2O_2, which was significantly faster than that observed in this study.[59] This increased efficiency may be ascribed to the direct use of liquid H_2O_2, which potentially enhanced the generation of reactive species, thereby accelerating the degradation rate. In contrast, Mohammadi and Pourmoslemi[60] reported a slightly lower k_1 value of 0.0040 min^{-1} for photocatalytic degradation using magnetic polymer-ZnO nanoparticles.

3.4. Possible Mechanism for DEX@nCPs(DEX)/Fe(II)/OA System. *3.4.1. Detection of Free Radicals.* Free radical scavenging tests were conducted using TBA and CF to identify the distinct contributions of $^{\bullet}OH$ and $^{\bullet}O_2^-$ radicals to the degradation of DOX in the DEX@nCPs(DEX)/Fe(II)/OA system. The reaction between TBA and $^{\bullet}OH$ radicals occurred at a significantly high rate constant ($kHO^{\bullet}$ = 5.2 × 108 M^{-1} s^{-1}), suggesting that TBA has a strong capacity to scavenge $^{\bullet}OH$ radicals. Furthermore, CF acts as an effective scavenger of $^{\bullet}O_2^-$ radicals owing to its significant rate constant with $^{\bullet}O_2^-$ radicals ($k^{\bullet}O_2^-$ = 3 × 1010 M^{-1} s^{-1}) and limited reactivity with $^{\bullet}OH$ radicals ($kHO^{\bullet}$ = 7 × 106 M^{-1} s^{-1}).[61,62] As shown in Figure 8, the addition of TBA significantly decreased DOX degradation efficiency from 88.9 to 10.4%. In contrast, the addition of 100 mM CF resulted in a decrease in DOX degradation efficiency from 88.9 to 52.6%. This indicates that $^{\bullet}O_2^-$ radicals also contribute to the breakdown of DOX in the DEX@nCPs(DEX)/Fe(II)/OA system, but to a lesser extent than $^{\bullet}OH$ radicals.

To validate the scavenging test involving $^{\bullet}OH$ radicals, the concentration of $^{\bullet}OH$ radicals in the DEX@nCPs(DEX)/Fe(II)/OA system was quantified using a fluorescence technique implemented according to a previously described method.[28] Fluorescence is a sensitive and reliable method for the detection of $^{\bullet}OH$ radicals. This method is based on the principle that $^{\bullet}OH$ radicals react with certain fluorescent dyes to produce fluorescent signals. The intensity of the fluorescence signal is proportional to the concentration of $^{\bullet}OH$ radicals in the system. As shown in Figure 9, the fluorescence technique provided compelling evidence for the presence of $^{\bullet}OH$ radicals in the DEX@nCPs(DEX)/Fe(II)/OA system. The observed increase in the fluorescence intensity over time is indicative of an increase in the concentration of $^{\bullet}OH$ radicals within the system. The increase in fluorescence intensity is also consistent with the expected behavior of the DEX@nCPs(DEX)/Fe(II)/OA system to constantly produce $^{\bullet}OH$ radicals.

3.4.2. Characterizations of Precipitates Generated after Optimization Studies. The FTIR spectra of the DEX@nCPs(DEX)/Fe(II)/OA precipitates, commercial CaO_2, oxalic acid, and iron(II) sulfate are shown in Figure 10. The peak at 1479 cm^{-1} in the commercial CaO_2 spectrum was assigned to O−Ca−O bending vibrations and carbonate ions, whereas the small peaks at 855−875 cm^{-1} were attributed to O−O stretching vibrations.[63] The prominent peak at 3414 cm^{-1} in the oxalic acid spectrum was assigned to the OH vibrations in the carboxylic acid functional group. The broad peak at 1225 cm^{-1} is associated with the C−O stretching vibrations of

Table 2. Comparison of Calcium-Based Materials and Methods of Antibiotic Degradation

study	materials	target pollutant	method	degradation efficiency (%)
Xu et al.[56]	nCPs	Tetracycline (TC)	ultrasonic waves	99.2
Xiang et al.[58]	nCPs	Sulfamethoxazole (SMX)	ozone	73.9
Bembibre et al.[57]	Ca-based nanoparticles	Tetracycline (TC)	photocatalytic	99.2
This study	DEX@nCPs(DEX)	Doxycycline (DOX)	fenton-like degradation	90.1

https://doi.org/10.1021/acsomega.4c09460
ACS Omega 2025, 10, 10205−10219

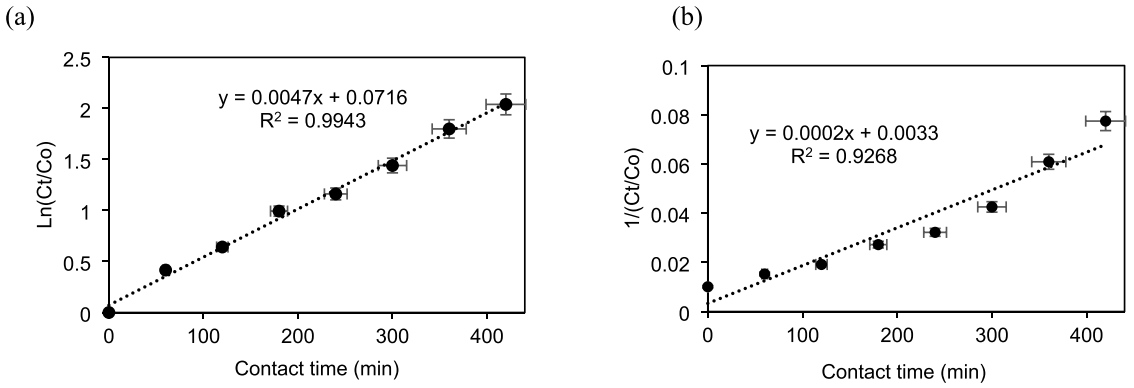

Figure 7. Kinetic plots of (a) first-order and (b) second-order DOX degradation in the DEX@nCPs(DEX)/Fe(II)/OA system. The experimental conditions were [DOX] = 10 mg/L, pH 5 using 0.1 M phosphate buffer, [Fe(II)] = 4 mM, [OA] = 6 mM, and [DEX@nCPs(DEX)] = 2 g/L.

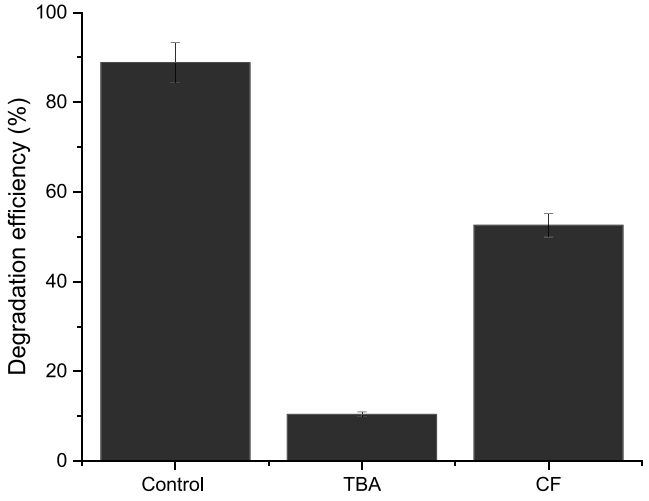

Figure 8. Degradation of DOX with different radical scavengers in the DEX@nCPs(DEX)/Fe(II)/OA system. The experimental conditions were [DOX] = 10 mg/L, pH = 5, [Fe(II)] = 0.004M, [OA] = 0.006M, and 2 g/L [DEX@nCPs(DEX)].

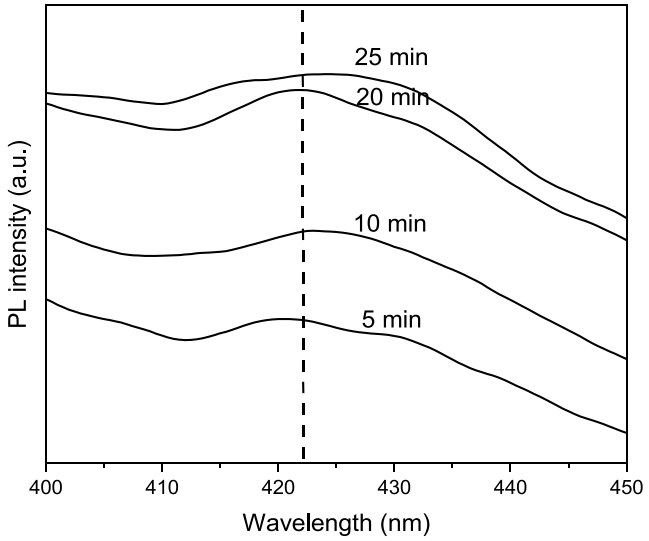

Figure 9. Quantification of •OH radicals by DEX@nCPs(DEX)/Fe(II)/OA at different contact times.

COO^- from the carboxylic acid group, and the significant peak at 1610 cm^{-1} corresponds to the C═O stretching vibrations of

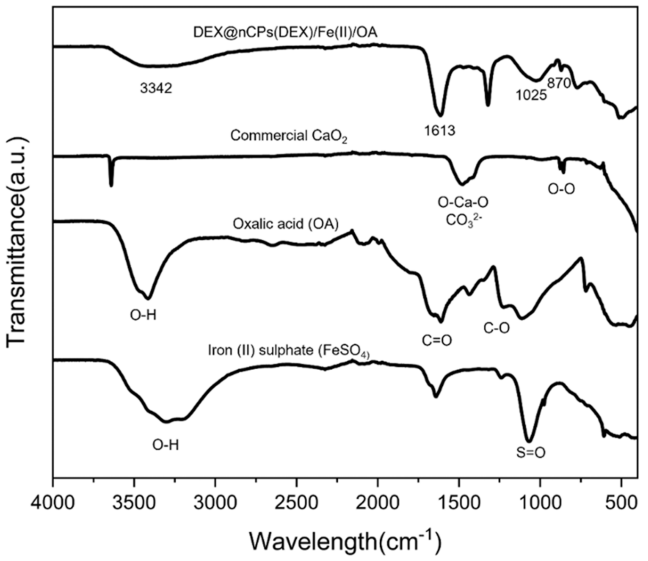

Figure 10. FTIR spectra of DEX@nCPs(DEX)/Fe(II)/OA precipitate, commercial CaO_2, oxalic acid and iron(II) sulfate.

oxalate.[64,65] For iron(II) sulfate, the broad peak at 3207−3301 cm^{-1} is likely associated with OH vibrations, which can be attributed to moisture. The intense peaks at 1068 cm^{-1} are the adsorption bands of S═O from the sulfate groups.[66,67]

Compared with the spectra of DEX@nCPs(DEX)/Fe(II)/OA, the prominent peak at 3342 cm^{-1} indicates OH stretching vibrations, suggesting the existence of OH groups from the alcohol functional groups originating from the dextran present in the complex, as described in our previous study.[21] In addition, the peak at 1613 cm^{-1} can be attributed to the stretching vibrations of the C═O bond, indicating the possible existence of oxalic acid. The prominent peak at 1025 cm^{-1} can be ascribed to the existence of C−O bonds derived from oxalic acid and sulfate groups originating from $FeSO_4$, as confirmed by EDX. In comparison with commercial CaO_2, the peaks corresponding to the O−Ca−O bonds at 1479 cm^{-1} disappeared, whereas smaller peaks associated with the O−O stretching vibrations at 870 cm^{-1} remained. These findings are consistent with those of Yuan et al.,[28] who reported the absence of CaO_2 after the degradation process, indicating that the precipitates likely consisted of $Ca(OH)_2$.

Figure 11a shows the SEM image of the DEX@nCPs-(DEX)/Fe(II)/OA precipitate after the degradation process, showing that it had irregular shapes. The EDX analysis in

https://doi.org/10.1021/acsomega.4c09460
ACS Omega 2025, 10, 10205−10219

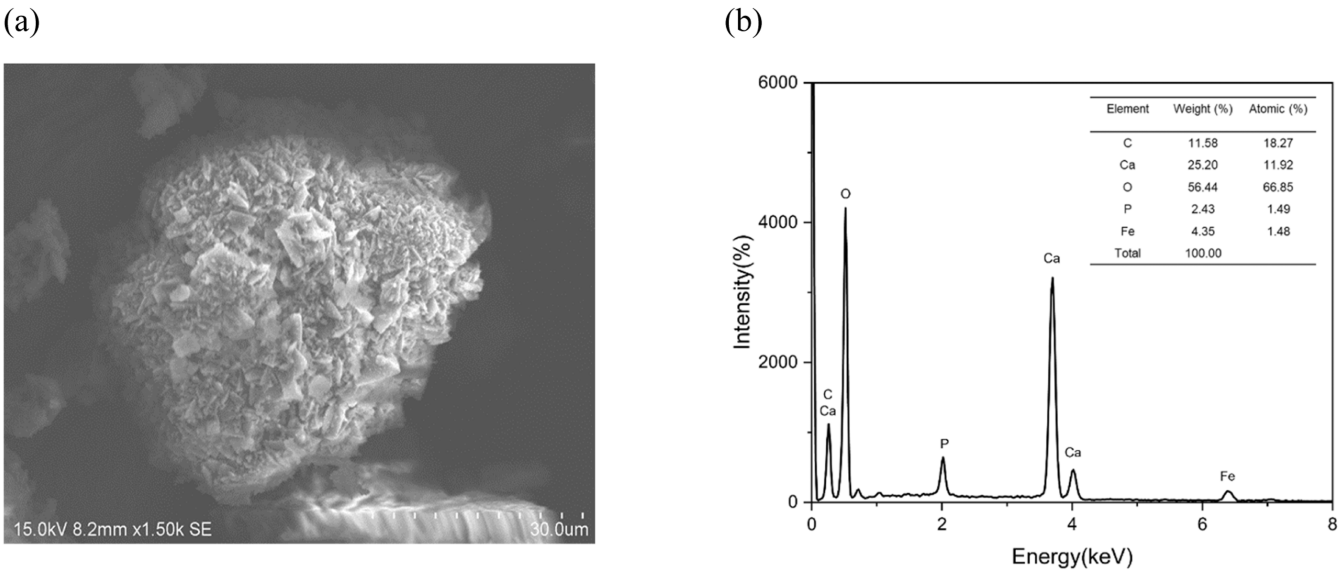

Figure 11. (a) SEM and (b) EDX images of the DEX@nCPs(DEX)/Fe(II)/OA precipitate generated after the optimization studies.

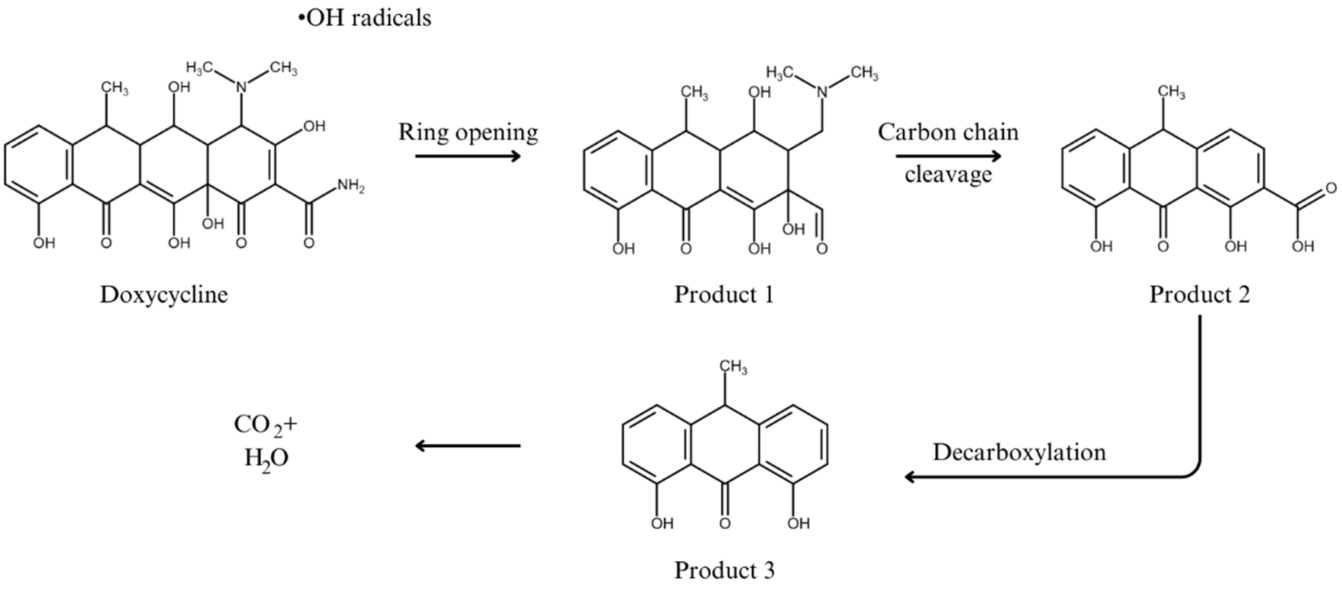

Figure 12. Proposed DOX degradation pathway via the DEX@nCPs(DEX)/Fe(II)/OA reaction.

Figure 11b reveals that the precipitate contained carbon (11.6%), calcium (25.2%), oxygen (56.4%), phosphorus (2.4%), and iron (4.4%). The presence of carbon indicates the presence of organic compounds, such as dextran coating on DEX@nCPs(DEX), whereas the presence of calcium suggests the incorporation of calcium ions from DEX@nCPs(DEX) into the precipitate.[21] The presence of phosphorus suggests the presence of phosphate-containing species, which is likely attributable to the phosphate buffer used during the reaction. The presence of iron confirms the involvement of Fe(II) in the reactions that contribute to the precipitate generation.

3.4.3. Proposed Degradation Pathway. When DEX@nCPs(DEX) are dissolved in water, they decompose into H_2O_2 according to eq 2. Fe(II) cleaves the weak O−O bond of H_2O_2 to generate •OH radicals (eq 5). Fe(II) acts as a catalyst and rapidly reacts with H_2O_2 to produce Fe(III) and OH, which have strong oxidizing properties. •OH radicals decomposed DOX, resulting in the formation of intermediate compounds, carbon dioxide, and water.

The proposed DOX degradation pathway under Fenton-like conditions provided valuable insights into the step-by-step breakdown of antibiotics (Figure 12). Degradation of DOX begins with •OH radical oxidation, resulting in the cleavage of aromatic rings and the formation of intermediate compounds (product 1).[68] Demethylation and carbon chain cleavage are important transformations that produce simpler molecules like organic acids (products 2 and 3).[69,70] These intermediates undergo further oxidation, resulting in the formation of CO_2 and H_2O.[21]

3.5. Environmental and Cost Analysis. DEX@nCPs-(DEX) offer significant potential for environmental protection due to their ability to controlled-release H_2O_2 and O_2 for long-term benefits. Given the significant potential of DEX@nCPs(DEX) in environmental applications, it addresses several Sustainable Development Goals (SDGs), including clean water

https://doi.org/10.1021/acsomega.4c09460
ACS Omega 2025, 10, 10205−10219

and sanitation (SDG 6), decent work and economic growth (SDG 8), climate action (SDG 13), and life on land (SDG 15). However, the introduction of DEX@nCPs(DEX) into the environment should only occur after thorough examination of their exact mechanism, toxicity, stability, residual analysis, and overall environmental impact on terrestrial and aquatic ecosystems.

Laboratory-scale production of DEX@nCPs(DEX) is challenging because of the low yield of DEX@nCPs(DEX), which can increase production costs. To facilitate commercialization or large-scale applications, it is critical to develop synthesis methods that increase the DEX@nCPs(DEX) yield, lower production costs, and increase profits. DEX@nCPs(DEX) can improve wastewater treatment efficiency, leading to cost savings and reduced need for additional chemical treatments.

4. CONCLUSIONS

This study showed that a heterogeneous Fenton-like system, which includes DEX@nCPs(DEX), Fe(II), and OA, can efficiently degrade DOX in water. The successful synthesis of DEX@nCPs (DEX) was confirmed using X-ray photoelectron spectroscopy (XPS). The optimal conditions (2 g/L DEX@nCPs(DEX), pH 5, 420 min) resulted in 90% DOX removal, which was 20% higher than that achieved using DEX@nCPs(DEX)/Fe(II) alone. The process had first-order kinetics (k_1 = 0.0047 min^{-1}), and model validation demonstrated high predictive accuracy (R^2 = 0.996; adjusted R^2 = 0.987). Scavenger and photoluminescence analyses identified $^{\bullet}OH$ as the primary reactive species, accounting for over 80% of the observed degradation.

This optimized DEX@nCPs(DEX)/Fe(II)/OA system provides a promising strategy for treating antibiotic-contaminated water, offering an efficient and sustainable approach for mitigating pharmaceutical pollutants and enhancing water quality. Further research should focus on real wastewater and the large-scale application of this system to establish viable treatments for pharmaceutical residues.

■ ASSOCIATED CONTENT

Supporting Information

The Supporting Information is available free of charge at https://pubs.acs.org/doi/10.1021/acsomega.4c09460.

Detailed experimental procedures (Text S1−S3); RSM-CCD design matrix and results (Table S1); ANOVA analysis (Table S2); overall desirability functions (Table S3); and experimental vs predicted degradation efficiency data (Table S4); H_2O_2 release profiles (Figure S1); calibration curves for doxycycline (Figure S2) and desirability ramp optimization (Figure S3) (PDF)

■ AUTHOR INFORMATION

Corresponding Authors

Nurul Nazihah Amerhaider Nuar − *Department of Chemistry, Faculty of Science, Universiti Putra Malaysia (UPM), Serdang, Selangor 43400, Malaysia;* orcid.org/0000-0002-7390-361X; Email: gs60035@student.upm.edu.my

Thomas Shean Yaw Choong − *Center of Sustainable Research, Department of Chemical and Environmental Engineering, Faculty of Engineering and Institute of Tropical Forest and Forest Products (INTROP), Universiti Putra Malaysia (UPM), Serdang, Selangor 43400, Malaysia;* Email: csthomas@upm.edu.my

Authors

Siti Nurul Ain Md Jamil − *Department of Chemistry, Faculty of Science, Universiti Putra Malaysia (UPM), Serdang, Selangor 43400, Malaysia; Centre for Foundation Studies in Science, Universiti Putra Malaysia (UPM), Serdang, Selangor 43400, Malaysia*

Syazana Ishami Mahadzir − *Department of Chemistry, Faculty of Science, Universiti Putra Malaysia (UPM), Serdang, Selangor 43400, Malaysia*

Intan Diana Mat Azmi − *Department of Chemistry, Faculty of Science, Universiti Putra Malaysia (UPM), Serdang, Selangor 43400, Malaysia; Centre for Foundation Studies in Science, Universiti Putra Malaysia (UPM), Serdang, Selangor 43400, Malaysia;* orcid.org/0000-0002-0168-3232

Mohd Salahuddin Mohd Basri − *Department of Process and Food Engineering, Faculty of Engineering, Universiti Putra Malaysia (UPM), Serdang, Selangor 43400, Malaysia*

Mohamad Rezi Abdul Hamid − *Center of Sustainable Research, Department of Chemical and Environmental Engineering, Faculty of Engineering, Universiti Putra Malaysia (UPM), Serdang, Selangor 43400, Malaysia*

Complete contact information is available at: https://pubs.acs.org/10.1021/acsomega.4c09460

Author Contributions

N.N.A.N.: Conceptualization, data curation, formal analysis, methodology, investigation, methodology, project administration, resources, software, validation, visualization and writing of the original draft. S.N.A.M.J.: Funding acquisition, resources, supervision, validation and writing−review and editing. T.S.Y.C.: Funding acquisition, resources, supervision, validation and writing−review and editing. S.I.M.: Investigation and methodology. I.D.M.A.: Supervision. M.S.M.B.: Software. M.R.A.H.: Funding acquisition.

Notes

The authors declare no competing financial interest.

■ ACKNOWLEDGMENTS

This research was funded by the Universiti Putra Malaysia under Geran Putra Inisiatif (GPI) (grant number: GPI/2023/9755200). The authors would like to acknowledge the Department of Chemistry, Faculty of Science, Universiti Putra Malaysia (UPM), and the Center of Sustainable Research Department of Chemical and Environmental Engineering, Faculty of Engineering, Universiti Putra Malaysia (UPM) for providing research facilities.

■ REFERENCES

(1) Emmanuel, W.-A.; Ewusie, E. A. Antibiotics in the Environment: Sources, Risks and Remedies. *Cent. Eur. Manage. J.* **2023**, *31*, 261−271, DOI: 10.57030/23364890.cemj.31.2.30.

(2) Akbari, M. Z.; Xu, Y.; Lu, Z.; Peng, L. Review of Antibiotics Treatment by Advance Oxidation Processes. *Environ. Adv.* **2021**, *5*, No. 100111.

(3) Zahoor, M.; Wahab, M.; Salman, S. M.; Sohail, A.; Ali, E. A.; Ullah, R. Removal of Doxycycline from Water Using Dalbergia Sissoo Waste Biomass Based Activated Carbon and Magnetic Oxide/Activated Bioinorganic Nanocomposite in Batch Adsorption and Adsorption/Membrane Hybrid Processes. *Bioinorg. Chem. Appl.* **2022**, *2022*, No. 2694487, DOI: 10.1155/2022/2694487.

(4) Moarefian, A.; Golestani, H. A.; Bahmanpour, H. Removal of Amoxicillin from Wastewater by Self-Made Polyethersulfone Membrane Using. *J. Environ. Health Sci. Eng.* **2014**, *12* (1), No. 127.
(5) Qalyoubi, L.; Al-Othman, A.; Al-Asheh, S. Removal of Ciprofloxacin Antibiotic Pollutants from Wastewater Using Nano-Composite Adsorptive Membranes. *Environ. Res.* **2022**, *215*, No. 114182.
(6) Chen, G.; Yu, Y.; Liang, L.; Duan, X.; Li, R.; Lu, X.; Yan, B.; Li, N.; Wang, S. Remediation of Antibiotic Wastewater by Coupled Photocatalytic and Persulfate Oxidation System: A Critical Review. *J. Hazard. Mater.* **2021**, *408*, No. 124461, DOI: 10.1016/j.jhazmat.2020.124461.
(7) Gul, S.; Hussain, S.; Khan, H.; Khan, K. I.; Khan, S.; Ullah, S.; Clasen, B. Advances in Bioremediation of Antibiotic Pollution in the Environment. In *Biological Approaches to Controlling Pollutants*; Elsevier, 2022; pp 49−78.
(8) Karim, M. A. H.; Aziz, K. H. H.; Omer, K. M.; Salih, Y. M.; Mustafa, F.; Rahman, K. O.; Mohammad, Y. Degradation of Aqueous Organic Dye Pollutants by Heterogeneous Photo-Assisted Fenton-like Process Using Natural Mineral Activator: Parameter Optimization and Degradation Kinetics. *IOP Conf. Ser.:Earth Environ. Sci.* **2022**, *958* (1), No. 012011, DOI: 10.1088/1755-1315/958/1/012011.
(9) Peng, X.; Yang, Y.; Wang, J.; Yuan, W.; Guo, Y.; Hu, W.; Yang, X. Cu/Fe Co-Modified Nitrogen Self-Doped Biochar as a Heterogeneous Fenton-like Catalyst for Degradation of Organic Pollutants: Synthesis, Performance, and Mechanistic Study. *J. Environ. Chem. Eng.* **2023**, *11* (5), No. 110866.
(10) Kakavandi, B.; Ahmadi, M.; Bedia, J.; Hashamfirooz, M.; Naderi, A.; Oskoei, V.; Yousefian, H.; Kalantary, R. R.; Pelalak, R.; Dewil, R. Metronidazole Degradation Mechanism by Sono-Photo-Fenton Processes Using a Spinel Ferrite Cobalt on Activated Carbon Catalyst. *Chemosphere* **2024**, *358*, No. 142102.
(11) Zhang, Q.; Peng, Y.; Peng, Y.; Zhang, J.; Yuan, X.; Zhang, J.; Cheng, C.; Ren, W.; Duan, X.; Xiao, X.; Luo, X. Mineralization versus Polymerization Pathways in Heterogeneous Fenton-like Reactions. *Water Res.* **2024**, *249*, No. 120931.
(12) Gokhale, D.; Chen, I.; Wu, W.; Gagnaire, A. M.; Doyle, P. S. A Zwitterionic Hydrogel-Based Heterogeneous Fenton Catalyst for Water Treatment. *Small* **2024**, *20*, No. 2402525, DOI: 10.1002/smll.202402525.
(13) Lin, S. M.; Yu, Y. L.; Zhang, Z. J.; Zhang, C. Y.; Zhong, M. F.; Wang, L. M.; Lu, S. X.; Xu, W.; Li, N.; Huang, X. The Synergistic Mechanisms of Citric Acid and Oxalic Acid on the Rapid Dissolution of Kaolinite. *Appl. Clay Sci.* **2020**, *196*, No. 105756.
(14) Ali, M.; Zhang, X.; Idrees, A.; Tariq, M.; Danish, M.; Farooq, U.; Shan, A.; Jiang, X.; Huang, J.; Lyu, S. Advancement in Fenton-like Reactions Using PVA Coated Calcium Peroxide/FeS System: Pivotal Role of Sulfide Ion in Regenerating the Fe(II) Ions and Improving Trichloroethylene Degradation. *J. Environ. Chem. Eng.* **2021**, *9* (1), No. 104591.
(15) Watcharadulyarat, N.; Rattanatayarom, M.; Ruangsawasdi, N.; Hongdilokkul, N.; Patikarnmonthon, N. Dextran-Based Nanoparticles for Encapsulation of Ciprofloxacin. *J. Phys.:Conf. Ser.* **2022**, *2175* (1), No. 012006.
(16) Predescu, A. M.; Matei, E.; Berbecaru, A. C.; Pantilimon, C.; Drăgan, C.; Vidu, R.; Predescu, C.; Kuncser, V. Synthesis and Characterization of Dextran-Coated Iron Oxide Nanoparticles. *R. Soc. Open Sci.* **2018**, *5* (3), No. 171525.
(17) Xue, Y.; Lu, S.; Fu, X.; Sharma, V. K.; Mendoza-Sanchez, I.; Qiu, Z.; Sui, Q. Simultaneous Removal of Benzene, Toluene, Ethylbenzene and Xylene (BTEX) by CaO2 Based Fenton System: Enhanced Degradation by Chelating Agents. *Chem. Eng. J.* **2018**, *331*, 255−264.
(18) Ma, X. H.; Zhao, L.; Dong, Y. H. Oxidation Degradation of 2,2′,5-Trichlorodiphenyl in a Chelating Agent Enhanced Fenton Reaction: Influencing Factors, Products, and Pathways. *Chemosphere* **2020**, *246*, No. 125849.
(19) Alrozi, R.; Zubir, N. A.; Bakar, N. F. A.; Motuzas, J.; Bakar, N. H. H. A.; Wang, D. Predicted Kinetic Behaviour of the Oxidative Degradation of Organic Pollutant Using Substituted MeCuFeO3 (Me = Ca, Sr, CaSr) Perovskite Catalysts. *ESTEEM Acad. J.* **2024**, *20*, 14−24.
(20) Xie, Z.-H.; He, C.-S.; Pei, D.-N.; Zheng, Y.-Z.; Wu, X.-Y.; Xiong, Z.; Du, Y.; Pan, Z.-C.; Yao, G.; Lai, B. Efficient Degradation of Micropollutants in CoCaAl-LDO/Peracetic Acid (PAA) System: An Organic Radical Dominant Degradation Process. *J. Hazard. Mater.* **2023**, *452*, No. 131286.
(21) Nuar, N. N. A.; Jamil, S. N. A. M.; Fan, L.; Azmi, I. D. M.; Pen-Chi, C.; Yaw, C. T. S. Synthesis of Controlled-Release Calcium Peroxide Nanoparticles Coated with Dextran for Removal of Doxycycline from Aqueous System. *Polymers* **2022**, *14* (18), No. 3866.
(22) Park, J. S.; Song, Y. J.; Lim, Y. G.; Park, K. Facile Fabrication of Oxygen-Releasing Tannylated Calcium Peroxide Nanoparticles. *Materials* **2020**, *13* (17), No. 3864.
(23) Beyan, S. M.; Prabhu, S. V.; Sissay, T. T.; Getahun, A. A. Sugarcane Bagasse Based Activated Carbon Preparation and Its Adsorption Efficacy on Removal of BOD and COD from Textile Effluents: RSM Based Modeling, Optimization and Kinetic Aspects. *Bioresour. Technol. Rep.* **2021**, *14*, No. 100664, DOI: 10.1016/j.biteb.2021.100664.
(24) Cheraghipour, E.; Pakshir, M. Environmentally Friendly Magnetic Chitosan Nano-Biocomposite for Cu(II) Ions Adsorption and Magnetic Nano-Fluid Hyperthermia: CCD-RSM Design. *J. Environ. Chem. Eng.* **2021**, *9* (2), No. 104883.
(25) Singh, J.; Nandabalan, Y. K. Copper(II) Bioremoval by a Rhizosphere Bacterium, Stenotrophomonas Acidaminiphila MYS1-Process Optimization by RSM Using Box−Behnken Design. *Int. J. Environ. Res.* **2017**, *11* (1), 63−70.
(26) Arabkhani, P.; Javadian, H.; Asfaram, A.; Hosseini, S. N. A Reusable Mesoporous Adsorbent for Efficient Treatment of Hazardous Triphenylmethane Dye Wastewater: RSM-CCD Optimization and Rapid Microwave-Assisted Regeneration. *Sci. Rep* **2021**, *11* (1), No. 22751.
(27) Moosazade, M.; Ashoori, R.; Moghimi, H.; Amani, M. A.; Frontistis, Z.; Taheri, R. A. Electrochemical Recovery to Overcome Direct Osmosis Concentrate-Bearing Lead: Optimization of Treatment Process via RSM-CCD. *Water* **2021**, *13* (21), No. 3136.
(28) Yuan, D.; Zhang, C.; Tang, S.; Li, X.; Tang, J.; Rao, Y.; Wang, Z.; Zhang, Q. Enhancing CaO2 Fenton-like Process by Fe(II)-Oxalic Acid Complexation for Organic Wastewater Treatment. *Water Res.* **2019**, *163*, No. 114861.
(29) Salari, M.; Nikoo, M. R.; Al-Mamun, A.; Rakhshandehroo, G. R.; Mooselu, M. G. Optimizing Fenton-like Process, Homogeneous at Neutral PH for Ciprofloxacin Degradation: Comparing RSM-CCD and ANN-GA. *J. Environ. Manage.* **2022**, *317*, No. 115469.
(30) Maachou, H.; Genet, M. J.; Aliouche, D.; Dupont-Gillain, C. C.; Rouxhet, P. G. XPS Analysis of Chitosan−Hydroxyapatite Biomaterials: From Elements to Compounds. *Surf. Interface Anal.* **2013**, *45* (7), 1088−1097.
(31) Butkus, B.; Havel, M.; Kostogiannes, A.; Howe, A.; Kang, M.; Gaume, R.; Richardson, K. A.; Banerjee, P. Calcium Sulfide Powder Analyzed by XPS. *Surf. Sci. Spectra* **2023**, *30* (1), No. 014005, DOI: 10.1116/6.0002304.
(32) Paparazzo, E. XPS Analysis of Oxides. *Surf. Interface Anal.* **1988**, *12* (2), 115−118.
(33) Aziz, M.; Ismail, A. F. X-Ray Photoelectron Spectroscopy (XPS). In *Membrane Characterization*; Elsevier, 2017; pp 81−93.
(34) Messele, S. A.; Bengoa, C.; Stüber, F. E.; Giralt, J.; Fortuny, A.; Fabregat, A.; Font, J. Enhanced Degradation of Phenol by a Fenton-like System (Fe/EDTA/H2 O2) at Circumneutral PH. *Catalysts* **2019**, *9* (5), No. 474.
(35) de Hoyos-Sifuentes, D. H.; Reséndiz-Hernández, P. J.; Díaz-Guillén, J. A.; Ochoa-Palacios, R. M.; Altamirano-Guerrero, G. Synthesis and Characterization of MgFe2O4 Nanoparticles and PEG-Coated MgFe2O4 Nanocomposite. *J. Mater. Res. Technol.* **2022**, *18*, 3130−3142.

https://doi.org/10.1021/acsomega.4c09460
ACS Omega 2025, 10, 10205−10219

(36) Ali, M.; Farooq, U.; Lyu, S.; Sun, Y.; Li, M.; Ahmad, A.; Shan, A.; Abbas, Z. Synthesis of Controlled Release Calcium Peroxide Nanoparticles (CR-NCPs): Characterizations, H2O2 Liberate Performances and Pollutant Degradation Efficiency. *Sep. Purif. Technol.* **2020**, *241*, No. 116729.
(37) Gankanda, A.; Rentz, N. S.; Greenlee, L. F. Influence of Ligand Size and Chelation Strength on Zerovalent Iron Nanoparticle Adsorption and Oxidation Behavior in the Presence of Water Vapor and Liquid Water. *J. Phys. Chem. C* **2019**, *123* (4), 2474−2487.
(38) Pignatello, J. J.; Oliveros, E.; MacKay, A. Advanced Oxidation Processes for Organic Contaminant Destruction Based on the Fenton Reaction and Related Chemistry. *Crit. Rev. Environ. Sci. Technol.* **2006**, *36*, 1−84.
(39) Tang, S.; Wang, Z.; Yuan, D.; Zhang, C.; Rao, Y.; Wang, Z.; Yin, K. Ferrous Ion-Tartaric Acid Chelation Promoted Calcium Peroxide Fenton-like Reactions for Simulated Organic Wastewater Treatment. *J. Cleaner Prod.* **2020**, *268*, No. 122253.
(40) Kaith, B. S.; Shanker, U.; Gupta, B.; Bhatia, J. K. RSM-CCD Optimized In-Air Synthesis of Photocatalytic Nanocomposite: Application in Removal-Degradation of Toxic Brilliant Blue. *React. Funct. Polym.* **2018**, *131*, 107−122.
(41) Mohagheghian, A.; Besharati-givi, N.; Ayagh, K.; Shirzad-siboni, M. Mineralization of Diazinon by Low-Cost CuO-Kaolin Nanocomposite under Visible Light Based RSM Methodology: Kinetics, Cost Analysis, Reaction Pathway and Bioassay. *J. Ind. Eng.Chem.* **2022**, *116*, 276−292.
(42) Issa, M. A.; Abidin, Z. Z.; Sobri, S.; Abdul-Rashid, S.; Mahdi, M. A.; Ibrahim, N. A.; Pudza, M. Y. Fabrication, Characterization and Response Surface Method Optimization for Quantum Efficiency of Fluorescent Nitrogen-Doped Carbon Dots Obtained from Carboxymethylcellulose of Oil Palms Empty Fruit Bunch. *Chin J. Chem. Eng.* **2020**, *28* (2), 584−592.
(43) Rauf, M. A.; Marzouki, N.; Körbahti, B. K. Photolytic Decolorization of Rose Bengal by UV/H2O2 and Data Optimization Using Response Surface Method. *J. Hazard. Mater.* **2008**, *159* (2−3), 602−609.
(44) Wu, J.; Zhang, H.; Oturan, N.; Wang, Y.; Chen, L.; Oturan, M. A. Application of Response Surface Methodology to the Removal of the Antibiotic Tetracycline by Electrochemical Process Using Carbon-Felt Cathode and DSA (Ti/RuO2-IrO2) Anode. *Chemosphere* **2012**, *87* (6), 614−620.
(45) Vijuksungsith, P.; Satapanajaru, T.; Chokejaroenrat, C.; Jarusutthirak, C.; Sakulthaew, C.; Kambhu, A.; Boonprasert, R. Remediating Oxytetracycline-Contaminated Aquaculture Water Using Nano Calcium Peroxide (NCaO2) Produced from Flue Gas Desulfurization (FGD) Gypsum. *Environ. Technol. Innovation* **2021**, *24*, No. 101861.
(46) Hung, C. M.; Chen, C. W.; Huang, C. P.; Dong, C. Di. Degradation of 4-Nonylphenol in Marine Sediments Using Calcium Peroxide Activated by Water Hyacinth (Eichhornia Crassipes)-Derived Biochar. *Environ. Res.* **2022**, *211*, No. 113076.
(47) Jiang, Y.; Ran, J.; Mao, K.; Yang, X.; Zhong, L.; Yang, C.; Feng, X.; Zhang, H. Recent Progress in Fenton/Fenton-like Reactions for the Removal of Antibiotics in Aqueous Environments. *Ecotoxicol. Environ. Saf.* **2022**, *236*, No. 113464.
(48) Zhang, Y.; Zhou, M. A Critical Review of the Application of Chelating Agents to Enable Fenton and Fenton-like Reactions at High PH Values. *J. Hazard. Mater.* **2019**, *362*, 436−450.
(49) Fiorentino, A.; Esteban, B.; Garrido-Cardenas, J. A.; Kowalska, K.; Rizzo, L.; Aguera, A.; Pérez, J. A. S. Effect of Solar Photo-Fenton Process in Raceway Pond Reactors at Neutral PH on Antibiotic Resistance Determinants in Secondary Treated Urban Wastewater. *J. Hazard. Mater.* **2019**, *378*, No. 120737.
(50) Honarmandrad, Z.; Javid, N.; Malakootian, M. Removal Efficiency of Phenol by Ozonation Process with Calcium Peroxide from Aqueous Solutions. *Appl. Water Sci.* **2021**, *11* (2), No. 14, DOI: 10.1007/s13201-020-01344-7.
(51) Northup, A.; Cassidy, D. Calcium Peroxide (CaO2) for Use in Modified Fenton Chemistry. *J. Hazard. Mater.* **2008**, *152* (3), 1164−1170.
(52) Xue, Y.; Gu, X.; Lu, S.; Miao, Z.; Brusseau, M. L.; Xu, M.; et al. The Destruction of Benzene by Calcium Peroxide Activated with Fe (II) in Water. *Chem. Eng. J.* **2016**, *302*, 187−193.
(53) Wu, J.; Jiang, Z.; Wan, L.; Song, H.; Abbass, K. Robust Optimization for Precision Product Using Taguchi-RSM and Desirability Function. *Arab J. Sci. Eng.* **2021**, *46* (3), 2803−2814.
(54) Mishra, S. K.; Ram, B. Steepest Descent Method. In *Introduction to Unconstrained Optimization with R*; Springer: Singapore, 2019; pp 131−173.
(55) Bokov, V. B. Statistical Method of Steepest Improvement of Response. *Ind. Lab. (Diagn. Mater.)* **2018**, *84* (11), 74−87.
(56) Xu, Z.; Sun, S.; Gao, M.; Zheng, R.; Mu, H.; Qiu, L.; Ma, J. Degradation of Tetracyclines via Calcium Peroxide Activation by Ultrasonic: Roles of Reactive Species, Oxidation Mechanism and Toxicity Evaluation. *Chemosphere* **2023**, *334*, No. 139033.
(57) Bembibre, A.; Benamara, M.; Hjiri, M.; Gómez, E.; Alamri, H. R.; Dhahri, R.; Serrà, A. Visible-Light Driven Sonophotocatalytic Removal of Tetracycline Using Ca-Doped ZnO Nanoparticles. *Chem. Eng. J.* **2022**, *427*, No. 132006.
(58) Xiang, L.; Xie, Z.; Guo, H.; Song, J.; Li, D.; Wang, Y.; Pan, S.; Lin, S.; Li, Z.; Han, J.; Qiao, W. Efficient Removal of Emerging Contaminant Sulfamethoxazole in Water by Ozone Coupled with Calcium Peroxide: Mechanism and Toxicity Assessment. *Chemosphere* **2021**, *283*, No. 131156.
(59) Sierra, R. S. C.; Zúñiga-Benítez, H.; Peñuela, G. A. Photo-Assisted Removal of Doxycycline Using H2O2 and Simulated Sunlight: Operational Parameters Optimization and Ecotoxicity Assessment. *J. Photochem. Photobiol., A* **2022**, *425*, No. 113697, DOI: 10.1016/j.jphotochem.2021.113697.
(60) Mohammadi, A.; Pourmoslemi, S. Enhanced Photocatalytic Degradation of Doxycycline Using a Magnetic Polymer-ZnO Composite. *Water Sci. Technol.* **2018**, *2017* (3), 791−801.
(61) Zhang, X.; Gu, X.; Lu, S.; Miao, Z.; Xu, M.; Fu, X.; Danish, M.; Brusseau, M. L.; Qiu, Z.; Sui, Q. Enhanced Degradation of Trichloroethene by Calcium Peroxide Activated with Fe(III) in the Presence of Citric Acid. *Front. Environ. Sci. Eng.* **2016**, *10* (3), 502−512.
(62) Chang, Y. Y.; Roh, H.; Yang, J. K. Improving the Clean-up Efficiency of Field Soil Contaminated with Diesel Oil by the Application of Stabilizers. *Environ. Technol.* **2013**, *34* (11), 1481−1487.
(63) Rastinfard, A.; Nazarpak, M. H.; Moztarzadeh, F. Controlled Chemical Synthesis of CaO2 Particles Coated with Polyethylene Glycol: Characterization of Crystallite Size and Oxygen Release Kinetics. *RSC Adv.* **2018**, *8* (1), 91−101.
(64) Mei, Y.; Wang, W.; Sun, H.; Nie, Z. Preparation and Morphology of Nano-Size Ceria by a Stripping Precipitation Using Oxalic Acid as a Precipitating Agent. *J. Rare Earths* **2012**, *30* (12), 1265−1269.
(65) Zhao, F.; Yan, F.; Qian, Y.; Xu, Y.; Ma, C. Roughened TiO2 Film Electrodes for Electrocatalytic Reduction of Oxalic Acid to Glyoxylic Acid. *J. Electroanal. Chem.* **2013**, *698*, 31−38.
(66) Labiapari, W. S.; Ardila, M. A. N.; Costa, H. L.; de Mello, J. D. B. Micro Abrasion-Corrosion of Ferritic Stainless Steels. *Wear* **2017**, *376*−*377*, 1298−1306.
(67) El-Yazeed, W. S. A.; El-Hakam, S. A.; Ibrahim, A. A.; Ahmed, A. I. Sulfated Iron Oxide Mesoporous Silica [SO42−/Fe2O3−MSiO2]: A Highly Efficient Solid Acid Catalyst for the Green Production of Pharmaceutically Significant 7-Hydroxy-4-Methyl Coumarin, 3,4-Dihydropyrmidinone and Hydroquinone Diacetate. *Inorg. Chem. Commun.* **2023**, *156*, No. 111174.
(68) Hong, P.; Li, Y.; He, J.; Saeed, A.; Zhang, K.; Wang, C.; Kong, L.; Liu, J. Rapid Degradation of Aqueous Doxycycline by Surface CoFe2O4/H2O2 System: Behaviors, Mechanisms, Pathways and DFT Calculation. *Appl. Surf. Sci.* **2020**, *526*, No. 146557.

(69) Tian, Y.; Liu, F.; Sun, B.; Tong, Z.; Fu, P.; Zhang, J.; Bi, W.; Xu, S.; Pei, G. Efficient Removal of Doxycycline Using Schwertmannite as a Heterogeneous Fenton-like Catalyst over a Wide PH Range. *J. Environ. Chem. Eng.* **2023**, *11* (2), No. 109441.
(70) Chen, J.; Huang, Z.; Wu, X.; Jiaqiang, E.; Leng, E. Experimental Investigation on Decomposition Characteristics of Doxycycline in Wastewater Using Hydrothermal Treatment: Exploring the Way to Complete Decomposition. *J. Environ. Chem. Eng.* **2023**, *11* (3), No. 109849, DOI: 10.1016/j.jece.2023.109849.

https://doi.org/10.1021/acsomega.4c09460
ACS Omega 2025, 10, 10205−10219